


V
AB

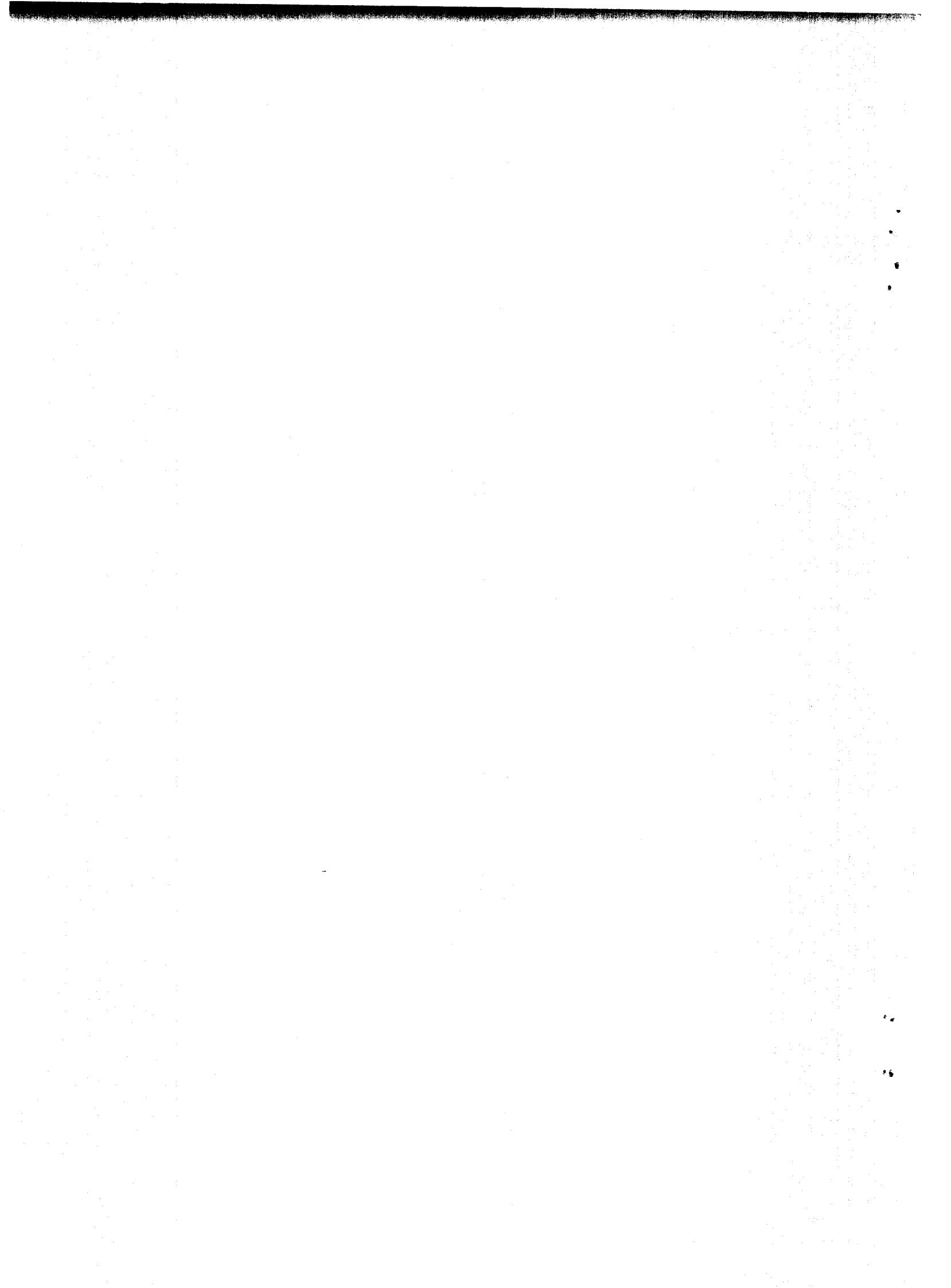
Nijmegen preprint
HEN-390
April 1996

**Two- and three-dimensional analysis of Bose-Einstein correlations in
 $\pi^+ / K^+ p$ interactions at 250 GeV/c**

EHS/NA22 Collaboration

SCAN-9605026

CERN LIBRARIES, GENEVA

SW8610



Two- and three-dimensional analysis of Bose-Einstein correlations in π^+/K^+ p interactions at 250 GeV/c

EHS/NA22 Collaboration

N.M. Agababyan⁷, M.R. Atayan⁷, M. Charlet^{4,a}, J. Czyzewski^{4,b}, E.A. De Wolf^{1,c}, K. Dziunikowska^{2,d},
A.M.F. Endler⁵, Z.Sh. Garutchava⁶, H.R. Gulkanyan⁷, R.Sh. Hakobyan⁷, J.K. Karamyan⁷,
D. Kisielewska^{2,d}, W. Kittel⁴, S.S. Mehrabyan⁷, Z.V. Metreveli⁶, E.C. Oliveira⁵, K. Olkiewicz^{2,d},
F.K. Rizatdinova³, E.K. Shabalina³, L.N. Smirnova³, M.D. Tabidze⁶, L.A. Tikhonova³, A.V. Tkabladze⁶,
A.G. Tomaradze^{6,e}, F. Verbeure¹, S.A. Zotkin³

¹ Department of Physics, Universitaire Instelling Antwerpen, B-2610 Wilrijk, Belgium

² Institute of Physics and Nuclear Techniques of Academy of Mining and Metallurgy and Institute of Nuclear Physics, PL-30055 Krakow, Poland

³ Nuclear Physics Institute, Moscow State University, RU-119899 Moscow, Russia

⁴ High Energy Physics Institute (HEFIN), University of Nijmegen/NIKHEF, NL-6525 ED Nijmegen, The Netherlands

⁵ Centro Brasileiro de Pesquisas Fisicas, BR-22290 Rio de Janeiro, Brazil

⁶ Institute for High Energy Physics of Tbilisi State University, GE-380086 Tbilisi, Georgia

⁷ Institute of Physics, AM-375036 Yerevan, Armenia

Abstract. The NA22 data on $\pi^-\pi^-$ correlations are analyzed in terms of a number of two- and three-dimensional parametrizations (Gaussian space-time, Goldhaber, Bowler string-like, Bertsch hydrodynamical, Kopylov-Podgoretskiĭ, etc.). Contrary to the results obtained for e^+e^- and $\mu\mu$ collisions, the Goldhaber parametrization, as well as string-like models, fail in describing the hadron-hadron data. Better fits are obtained in the framework of surface-emitting fireball-like models, both when including and excluding hydrodynamical expansion of nuclear matter. Our results indicate that pion radiation occurs at earlier stages of matter evolution than in nuclear collisions.

^a EC guest scientist, now at DESY, Hamburg

^b KUN Fellow from the Jagellonian University, Krakow, and Fellow of the Polish Science Foundation (FNP) scholarship for the year 1996

^c Onderzoeksleider NFWO, Belgium

^d Supported by the Polish State Committee for Scientific Research

^e Now at UIA, Wilrijk, Belgium

1 Introduction

Boson interferometry provides a powerful tool for the investigation of the space-time structure of particle-production processes (for recent reviews see [1-5]). The Bose-Einstein correlations (BEC) of two identical bosons at small four-momentum difference, $q = p_1 - p_2$, reflect both geometrical and dynamical properties of the particle-radiating source. In an over-simplified picture, one assumes the source to consist of motionless (in the source rest frame) point-like emitters which radiate identically (independently of their space-time coordinates). The two-particle correlation function depends, therefore, only on q and relates directly to the square of the Fourier transform of the space-time density distribution of emitters, thus providing a measurement of the size, shape and radiation time of the source [1-5].

This simple geometrical interpretation of the interference pattern can be invalid when emitters move at relativistic velocities with respect to each other, leading to strong dynamical correlations between space-time and momentum-energy coordinates of emitted particles. Dynamical correlations of this type are inherent for expanding sources, such as a color string in lepton-induced reactions [6] or a longitudinally expanding central fireball in ultrarelativistic nuclear collisions [7]. The interplay between geometrical and dynamical effects alters the interference pattern. This influence on the BEC is considered in the framework of the color string ([8-10] and refs. therein) and hydrodynamical ([11-23] and refs. therein) models. In the general case of a dynamic source, the two-particle correlations are described as a function of five independent kinematical variables: the three components of the vector \mathbf{q} and the two components (assuming azimuthal symmetry of the interaction) of the sum vector $\mathbf{p} = \mathbf{p}_1 + \mathbf{p}_2$ (e.g. the longitudinal p_L and transverse $|\mathbf{p}_T|$ components). However, under certain simplifying assumptions, the correlation function can be parametrized with a reduced number of kinematical variables.

In this work, an attempt is undertaken to distinguish between an expanding (string-like or hydrodynamical) and a non-expanding (fireball-like) pattern of multiparticle production in hadronic reactions. This attempt is executed by means of an experimental study of the two- and three-dimensional BEC of pairs of negative pions in $(\pi^+/K^+)p$ interactions at 250 GeV/c. The sets of two- and three-dimensional variables and parametrizations of the correlation function used in this analysis are given in Sect. 2. Experimental results are presented in Sect. 3 and conclusions are summarized in Sect. 4.

2 Variables and parametrizations

The following pairs or triplets of variables are used for the two- and three-dimensional analyses:

- a) $|\mathbf{q}|$ versus q_0 , where $\mathbf{q} = \mathbf{p}_1 - \mathbf{p}_2$ and $q_0 = |E_1 - E_2|$ are, respectively, the momentum and energy difference of the two identical pions (in the CMS).
- b) The Lorentz-invariant variables Q_L^2 versus Q_T^2 , where \mathbf{Q}_T is the component of \mathbf{q} perpendicular to the collision axis, and $Q_L^2 = q_L^2 - q_0^2$, where q_L^2 is the component of \mathbf{q} parallel to the collision axis.
- c) $q_L (= |q_L|)$ versus $Q_T (= |\mathbf{Q}_T|)$ and q_L versus Q_{To} and Q_{Ts} , where Q_{To} is the 'out' component of \mathbf{Q}_T parallel to pair transverse momentum $\mathbf{p}_T = \mathbf{p}_{T1} + \mathbf{p}_{T2}$ and Q_{Ts} is the 'side' component of \mathbf{Q}_T perpendicular to \mathbf{p}_T (see Fig. 1):

$$Q_{To} = \frac{\mathbf{Q}_T \cdot \mathbf{p}_T}{|\mathbf{p}_T|} \quad Q_{Ts} = \frac{|\mathbf{Q}_T \times \mathbf{p}_T|}{|\mathbf{p}_T|}$$

d) $q_T (= |\mathbf{q}_T|)$ versus q_0 , where \mathbf{q}_T is the component of \mathbf{q} perpendicular to $\mathbf{p} = \mathbf{p}_1 + \mathbf{p}_2$ (in the CMS).

The following parametrizations are used for the normalized two-particle density:

$$R(\mathbf{p}_1, \mathbf{p}_2) = \frac{\rho(\mathbf{p}_1, \mathbf{p}_2)}{\rho_1(\mathbf{p}_1)\rho_1(\mathbf{p}_2)} .$$

1. The Gaussian form

$$R(\mathbf{q}^2, q_0^2) = \gamma[1 + \lambda \exp(-\beta_1 \mathbf{q}^2 - \beta_2 q_0^2)](1 + \delta \mathbf{q}^2 + \epsilon q_0^2) . \quad (1)$$

In (1), $\lambda \leq 1$ is the coherence parameter, γ is an overall normalization and $(1 + \delta \mathbf{q}^2 + \epsilon q_0^2)$ is introduced to account for a possible slow variation of R outside the interference peak.

At $\beta_1, \beta_2 > 0$, these two parameters are related, respectively, to the mean radius and the mean radiation time of a fireball-like (volume emitting) source with a Gaussian space-time distribution. At negative β_2 , and $\beta \equiv \beta_1 = -\beta_2$, (1) reduces to the Goldhaber parametrization [24]

$$R(\mathbf{q}^2, q_0^2) = \gamma[1 + \lambda \exp(-\beta Q^2)](1 + \delta Q^2) \quad (2)$$

with the Lorentz-invariant variable $Q^2 = \mathbf{q}^2 - q_0^2$ and a parameter β related to the r.m.s. radius ($\beta = r^2/3$) of a source being of a spherically symmetric Gaussian form in the dipion rest frame.

2. The Bowler parametrizations for a string-like source [8,10]:

$$R(Q_L^2, Q_T^2) = \gamma[1 + \lambda \exp(-\beta_L Q_L^2 - \beta_T Q_T^2)](1 + \delta Q_L^2 + \epsilon Q_T^2) \quad (3)$$

and

$$R(Q_L^2, Q_T^2) = \gamma \left[1 + \frac{A}{2[(\beta_L Q_L^2)^2 - 1]} \ln(\beta_L |Q_L^2|) \exp(-\beta_T Q_T^2) \right] (1 + \delta |Q_L^2| + \epsilon Q_T^2) , \quad (4)$$

where β_L and β_T correspond to the longitudinal and transverse size of the string segment radiating the BE correlated pions, respectively. The parameter A has the definition of $A = 1/|y_{\max}|$, where y_{\max} is the maximum rapidity y , above which the y distribution drops rapidly.

3. The two- and three-dimensional Gaussian parametrizations used for a hydrodynamically expanding cylindrical source (see e.g. [13,15,19,21,22,23]):

$$R(q_L, Q_T) = \gamma[1 + \lambda \exp(-\frac{1}{2} r_L^2 q_L^2 - \frac{1}{2} r_T^2 Q_T^2)](1 + \delta q_L + \epsilon Q_T) \quad (5)$$

$$R(q_L, Q_{To}, Q_{Ts}) = \gamma[1 + \lambda \exp(-\frac{1}{2} r_L^2 q_L^2 - \frac{1}{2} r_o^2 Q_{To}^2 - \frac{1}{2} r_s^2 Q_{Ts}^2 + r_{o,L}^2 Q_{To} q_L)] \times \quad (6)$$

$$\times (1 + \delta q_L + \epsilon Q_{To} + \xi Q_{Ts}) ,$$

where r_L, r_T, r_o, r_s are, respectively, the longitudinal (along the cylinder axis), transverse, 'out' and 'side' effective dimensions of the source segment radiating the BE correlated pion pairs, while $r_{o,L}$ represents an "out-longitudinal" cross term recently introduced in [22] and, depending on the particular emission model, corresponding to e.g. the duration of particle emission. In comparing our results to those of other experiments, it is important to note that some authors use (5) and (6) without the factors 1/2 in the exponents.

4. The Kopylov-Podgoretskiĭ parametrization [25]:

$$R(q_T, q_0) = \gamma \left[1 + \lambda \left[\frac{2J_1(\tau_K q_T)}{(\tau_K q_T)} \right]^2 (1 + \tau^2 q_0^2)^{-1} \right] (1 + \delta q_T + \epsilon q_0), \quad (7)$$

where J_1 is the first-order Bessel function and where τ_K is the radius of a surface-emitting spherical source decaying exponentially with the mean time τ .

3 The results

The data were obtained from the NA22 experiment, performed at the CERN SPS with the help of the European Hybrid Spectrometer [26]. Recent results concerning BEC in π^+p and K^+p collisions in the same experiment are published in [27,28,29,30], where the experimental procedure is described in detail. A related, but alternative analysis in terms of an inverse power-law behavior of R is presented in Fig. 20 of [31].

The results of this paper are based on an analysis of about 140k events of $(\pi^+/K^+)p$ interactions at 250 GeV/c, including 101.147 events containing at least two negative tracks with momentum resolution better than 4%. (Depending on the momentum, the average momentum resolution varies from 1 % to 2.5 %). All negative particles are assumed to have pion mass. The contamination from other particles is estimated to be $(7 \pm 3)\%$. Each accepted track is required to lie in the region of Feynman variable $|x_F| < 0.5$, in order to reduce possible correlations due to phase space restriction, as well as biases due to violation of energy and momentum violation imminent to the mixed-event technique. Single diffraction dissociation is excluded. For each event, a weight is introduced in order to normalize to the non-single diffractive topological cross sections. The number of $\pi^-\pi^-$ combinations exceeds half a million (542.554).

Experimentally, the normalized two-particle densities R are determined as the ratio of the number of pairs (at given values of the kinematical variables) to that of the reference (background) sample composed by combining tracks randomly chosen from different events of the same charged particle multiplicity. The fraction of a given multiplicity in the reference sample is equal to that in the real event sample. Both samples are normalized to an equal number of combinations in the whole interval of variation of the corresponding kinematical variables.

Below, we present the results of the analysis of BEC using the different sets of variables for the two- and three-dimensional analyses described in Sect. 2.

3.1 q^2 versus q_0^2

The normalized two-dimensional distribution in the variables q^2 and q_0^2 is shown in Figs. 2a and 2b for two different ranges and scales. Note, that the large deviations of the ratio $R(q^2, q_0^2)$ from unity in the region of relatively large q^2 and q_0^2 ($> 0.3 \text{ GeV}^2$) are due to statistical fluctuations and, therefore, have large errors.

The fit results of $R(q^2, q_0^2)$ obtained according to parametrization (1) are presented in Table 1 for two different ranges and binnings in the variables q^2 and q_0^2 . The fit leads to a negative value of the parameter β_2 , thus excluding a volume-emitting fireball-like source of spherically symmetric Gaussian space-time distribution.

On the other hand, the absolute value of β_2 is much smaller than the value of β_1 . A fit under the condition $\beta \equiv \beta_1 = -\beta_2$ (parametrization (2)) results in too large a χ^2 ($\chi^2/NDF = 846/321$ and $1468/321$ for the data presented in Figs. 2a and 2b, respectively). Two crucial tests for parametrization

(2) are presented in Figs. 2c and 2d. Fig. 2c shows the dependence of $R(\mathbf{q}^2, q_0^2)$ on \mathbf{q}^2 along the diagonal $\mathbf{q}^2 \approx q_0^2$, i.e., at fixed $Q^2 = \mathbf{q}^2 - q_0^2 \approx 0$. While parametrization (2) predicts no \mathbf{q}^2 -dependence at fixed Q^2 , the data exhibit a strong \mathbf{q}^2 -dependence. Fig. 2d shows the Q^2 -dependence of $R(\mathbf{q}^2, q_0^2)$ integrated over the region $\mathbf{q}^2, q_0^2 > 0.8 \text{ GeV}^2$. In the framework of fireball-like models (with independent space- and decay-time distributions of emitters within the fireball volume or on the fireball surface), no interference effects are expected at large \mathbf{q}^2 and/or q_0^2 . On the other hand, parametrization (2) predicts an interference enhancement at small Q^2 , irrespective of the values of \mathbf{q}^2 and q_0^2 . Our data exclude the applicability of (2) to the region of large \mathbf{q}^2 and q_0^2 .

Our data shown in Fig. 2 are in contrast with those obtained in the hard processes of e^+e^- -annihilation [32] and muon-nucleon scattering [33]. In these types of collisions, the extracted parameters β_1 and β_2 satisfy the relation $\beta \equiv \beta_1 \approx -\beta_2$ ($\beta \approx 10.5 \text{ GeV}^{-2}$ in [32] and $\beta \approx 2.2 \text{ GeV}^{-2}$ in [33]), and the interference effects observed at large \mathbf{q}^2 and q_0^2 ($> 0.8 \text{ GeV}^2$) are completely in accordance with those observed for the full sample of events [33]. We, therefore, conclude that the space-time evolution of multiparticle production is different in hadron- and lepton-induced reactions.

3.2 Q_L^2 versus Q_T^2

The dependence of the ratio R on Q_L^2 and Q_T^2 is plotted in Fig. 3. One can see that, at least at small Q_T^2 , for which our data are statistically more abundant, the ratio $R(Q_L^2, Q_T^2)$ is enhanced at $Q_L^2 \sim 0$. This enhancement does not grow as Q_L^2 becomes negative. This behavior is in contrast with that found in the e^+e^- [32] and $p\bar{p}$ [34] data, where, in accordance with the string fragmentation picture [10], an increase of the ratio R is observed for negative Q_L^2 .

The fit according to the Bowler parametrization (3) results in too low a confidence level (Table 2). The results of the fit are plotted in Fig. 3b-3p. The agreement with the data is worst at $Q_L^2 < 0$ due to the exponential rise of the curves corresponding to (3), although a separate fit of the data at positive Q_L^2 improves the description only slightly (Table 2). Only the data at $Q_L^2 < 0$ cannot be fitted by (3).

The first two lines of Table 3 present the fit results according to parametrization (4). The description of the data is bad for both intervals of $-0.5 \leq Q_L^2 \leq 0.5 \text{ GeV}^2$ and $0 \leq Q_L^2 \leq 0.5 \text{ GeV}^2$. Only the data at $Q_L^2 < 0$ cannot be fitted by (4). A satisfactory description (CL $\approx 5\%$) by parametrization (4) is achieved for the ratio R as a function of Q_T^2 and the modulus $|Q_L^2|$, plotted in Fig. 4. The parameter values $\beta_L = 10.1 \pm 1.7 \text{ GeV}^{-2}$ and $A = 0.37 \pm 0.03$ are within the range predicted [8]. The parameter β_T , characterizing the transverse size of the string, is not predicted in the model [8]. Our estimate of the transverse size, $r_T = 0.60 \pm 0.03 \text{ fm}$, agrees with $r_T = 0.64 \pm 0.07 \text{ fm}$ [24] extracted from the e^+e^- data.

Contrary to the results presented in this and the previous subsection, an acceptable fit to the same data by the Goldhaber parametrization (2) was obtained in previous analysis [28]. The Goldhaber formula, however, does not consider the space and time variables (or, alternatively, the longitudinal and transverse variables) separately. The Goldhaber formula was applied in [28] to fit our *one-dimensional* Q^2 data, which in fact are obtained by means of integration of two-dimensional data over q and q_0 (at fixed $Q^2 = \mathbf{q}^2 - q_0^2$, see (1)) or, alternatively over Q_L and Q_T (at fixed $Q^2 = Q_L^2 + Q_T^2$, see (3)). The *two-dimensional* parametrizations (1) or (3) could be reduced to parametrization (2) if $\beta_1 = -\beta_2$ in (1) or $\beta_L = \beta_T$ in (3), i.e., if (in the framework of the string-like model) the longitudinal and transverse sizes of the string segment (radiating the BE correlated pions) were equal. Our data show that this is not the case. The acceptable fit of the one-dimensional data with (2) in [28] allows us to extract an averaged (over the dipion rest frames) r.m.s. radius of the source assumed to be of a spherically symmetric Gaussian form in the dipion rest frame. It does not necessarily mean an acceptable fit of the two-dimensional data with $\beta_1 = -\beta_2$ in (1) or $\beta_L = \beta_T$ in (3).

3.3 q_L versus Q_T and q_L versus Q_{T0} and Q_{Ts}

In this subsection we present the results of the analysis of BE correlation in the framework of hydrodynamical models describing the space-time evolution of a centrally produced hadronic fireball. The evolution pattern includes the thermalization of the hadron matter at some proper time τ , its longitudinal expansion (along the collision axis), and final breakup at a final (freeze-out) temperature T_f . For a centrally produced pion pair with an average rapidity $|y| = \frac{1}{2}|y_1 + y_2| < Y$ (below the value $Y = 1.5$ in the CMS is used) the Bose-Einstein correlation can be approximately parametrized as (5) [19]. In contrast with the case of a non-expanding source for a longitudinally expanding source the parameter r_L in (5) is not a constant, but depends strongly on y and the average transverse mass of the two pions, $m_T = \frac{1}{2}(m_{T1} + m_{T2})$ [15,19]:

$$r_L(y) = \frac{\tau(y)}{ch y} \sqrt{\frac{2T_f}{m_T}}, \quad (8)$$

where the parameter $\tau(y) = \tau_f = const$ is the proper time of thermalization for the Bjorken scaling model [7]. For the Landau non-scaling model (see [14]) the parameter $\tau(y)$ has the definition of an inverse gradient of the longitudinal four-velocity of the hydrodynamical flow, $\tau(y) = (du_L/dx_L)^{-1}$, and may slightly depend on y (for the hydrodynamical models $\tau(y) \leq \tau(0)$). Recently, the hydrodynamical formula (8) has experimentally been verified by results from pion and kaon interferometry in nuclear collisions at 200 GeV per nucleon [35,36,37].

The dependence of the ratio R on q_L and Q_T is plotted in Fig. 5 and the fit results according to parametrization (5) are presented in Table 4. The observed effective longitudinal size of $r_L = 1.23 \pm 0.06$ fm significantly exceeds the transverse size of $r_T = 0.89 \pm 0.04$ fm.

The effective longitudinal size r_L at different y , shown in Fig. 6a, demonstrates a behavior consistent with the $(ch y)^{-1}$ dependence predicted by (8) (the dashed curve). Note that p_T dependence on y is negligible and the average transverse mass $\langle m_T \rangle$ is practically the same ($\langle m_T \rangle = 0.36 \div 0.37$ GeV/ c^2) in all intervals of y considered.

The observed dependence $r_L(y)$ is expected to disappear (at $\tau(y) = const$) or to be reduced (at $\tau(y) \neq const$) in the so-called longitudinal CMS (LCMS) [38], in which the longitudinal momentum sum is zero, i.e., $y^* = \frac{1}{2}(y_1^* + y_2^*) = 0$. This expectation is confirmed by the results of our analysis in the LCMS (Fig. 6b), indicating that the parameter $\tau(y)$ is almost independent of y (the average rapidity of the pion pair in the CMS).

The data at $|y| < 1.5$ were analyzed in the LCMS in two different regions, $m_T < 0.35$ GeV (with $\langle m_T \rangle = 0.26 \pm 0.05$ GeV) and $m_T = 0.35 \div 1$ GeV (with $\langle m_T \rangle = 0.45 \pm 0.09$ GeV). The results presented in Table 5 show a decrease of the parameters r_L and r_T with increasing m_T . The variation of r_L is consistent with the $1/\sqrt{m_T}$ dependence predicted by the hydrodynamical formula (8). Assuming the hadronization temperature to be of order $T_f \sim m_\pi \approx 140$ MeV, and using $r_L \sqrt{m_T} = 0.67 \pm 0.07$ GeV^{1/2}fm from Table 5, one can estimate the parameter

$$c\tau(y) \approx c\tau(0) = r_L \sqrt{\frac{m_T}{2T_f}} = 1.3 \pm 0.2 \text{ fm}, \quad (9)$$

which, being almost independent of y , can be considered as the source-thermalization proper time τ_f at which the source breaks up instantly into pions.

In agreement with an unexpected observation of [36], we find (last column of table 5) that r_T is also compatible with an $\sqrt{m_T}$ scaling. In [21,23,39] this scaling has been related to a transverse expansion and/or transverse gradient of the local temperature for a cylindrically symmetric, longitudinally expanding finite source.

A more general scenario of the hydrodynamical evolution of hadronic matter includes the transverse expansion of the hydrodynamical tube and a non-vanishing duration time $\Delta\tau_f$ of the pion emission at the freeze-out temperature T_f [21,38]. In this case, the interference pattern can be described by the three-dimensional dependence (6) (rather than the two-dimensional (5)), where the 'out' and 'side' interferometric radii r_o and r_s may differ. For example, in the case of non-relativistic transverse hydrodynamical flow, the effective radius r_o along the dipion transverse momentum \mathbf{p}_T is sensitive to the duration time $\Delta\tau_f$ and exceeds the radius r_s (perpendicular to \mathbf{p}_T) which measures the geometrical transverse size of the hydrodynamical tube. Under the assumption that the freeze-out time τ_f obeys a Gaussian distribution of width $\Delta\tau_f < \tau_f$, the following relation holds [38]:

$$r_o^2 = r_s^2 + 2(v_T \Delta\tau_f)^2, \quad (10)$$

where v_T is the transverse pion-pair velocity in the LCMS, the average value of which is estimated from our data as $v_T = 0.484c$.

The results of the three-dimensional fit by parametrization (6) in the LCMS are presented in the first line of Table 6. The fit results in $r_L > r_o > r_s$. The value of $r_{o,L}$ is of the same size as that of r_s , but its statistical significance is less than 3 standard deviations. For that reason, and to be able to compare our results to earlier ones [37], we repeat the fit after fixing $r_{o,L}$ at value 0.0. The results are given in the second line of Table 6 and do not differ from the first line outside errors. Projections onto the three axes are shown in Fig. 7, using 40 MeV cuts on the non-projected components. Note that the quoted 'side' radius $r_s = 0.76 \pm 0.10$ fm is close to the proton radius. Using the results of Table 6 and the average transverse velocity $v_T = 0.484c$, one obtains from (10): $c\Delta\tau_f = 1.3 \pm 0.3$ fm, i.e., $\Delta\tau_f \sim \tau_f$. The quoted value of $\Delta\tau_f$ does not satisfy the condition $\Delta\tau_f < \tau_f$ which is necessary for the validity of (10). Nevertheless, if $\Delta\tau_f$ could be accepted as a rough estimate of the duration time of pion radiation, then a possible interpretation of $\Delta\tau_f \sim \tau_f$ might be that the radiation process occurs during all the hydrodynamical evolution of the hadronic matter. This pattern is in contrast with that observed in nuclear collisions for which the duration time is found to be much shorter ($c\Delta\tau_f < 2$ fm) than the freeze-out time $c\tau_f \sim 4$ fm [37].

Another distinction between interferometric data in hadronic and nuclear collisions is revealed when comparing the ratio of the freeze-out volume (proportional to $r_s^2 r_L$) and the density of pions $\rho(y) = d\langle n_- \rangle / dy$ in the central rapidity region. In nuclear collisions, this ratio is found [37] to be $k = r_s^2 r_L / \rho(y) = 2.00 \pm 0.15$ fm³ for all considered combinations of colliding nuclei (with atomic number varying from 12 to 197). As concluded in [37], the constancy of k indicates that the hadronic matter breaks up and radiates pions at constant particle density (inversely proportional to k). In our experiment, $r_s^2 r_L = 1.01 \pm 0.29$ fm³ and the density in the central rapidity region ($|y| < 1.5$) is $\rho(y) = 0.910 \pm 0.003$ for the sample with two or more π^- mesons. The ratio $k = 1.1 \pm 0.3$ fm³ is smaller than that for the nuclear data, indicating that in hadronic collisions the pion radiation occurs during earlier stages of matter evolution and at higher densities than in nuclear collisions.

In lines 3 and 4 of Table 6, the fits according to (6) are repeated in two charged particle multiplicity ranges. For $n < 10$ [$\rho(y) = 0.500 \pm 0.001$] and $n \geq 10$ [$\rho(y) = 1.120 \pm 0.002$], we obtain $k = 1.3 \pm 0.5$ and 1.0 ± 0.3 , respectively. Therefore, here also, k does not depend on the density, even though such a dependence cannot be excluded because of the large statistical errors.

It is interesting to compare our results related to the transverse evolution of the hadronic matter with predictions of the Bjorken hadronization picture of an expanding shell [40]. The latter is supposed to be a single layer of closely packed pions. Just after the hadronization, the average differential multiplicity $d\langle n \rangle / dy d\varphi$ (per unit of rapidity and azimuthal angle) of pions, seen in the reference frame where they emerge at 90° , is related to the squared transverse radius of the source shell at the

hadronization time:

$$R_h^2 = (1.2\text{fm})^2 \frac{d\langle n \rangle}{dyd\varphi}. \quad (11)$$

Assuming $\langle n \rangle = 3\langle n_- \rangle$, we obtain: $d\langle n \rangle/dyd\varphi = 0.434$, and $R_h = 0.79\text{fm}$. This result agrees with the 'side' radius $r_s = 0.76 \pm 0.10\text{fm}$ (Table 6) measured in the LCMS where a pion pair emerges at 90° .

The thickness of the shell predicted in [40] is between $0.2 - 0.4\text{fm}$ (if the collision has occurred between only one pair of constituent quarks) and $0.5 - 1.5\text{fm}$ (if more than one pair of quarks has participated in the collision). On the other hand, the finiteness of the shell thickness can be attributed to the non-vanishing duration time of hadronization and the transverse flow of pion pairs, which lead to a non-vanishing difference between 'out' and 'side' radii, $r_o - r_s = 0.42 \pm 0.16\text{fm}$ (see Table 6). This difference, which can be considered an effective thickness of the radiating shell, is within the range predicted in [37].

3.4 q_T versus q_0

The ratio $R(q_T, q_0)$ is shown in Fig. 8. The fit results according to parametrization (7) for $q_T < 1$ GeV and different ranges of the variable q_0 (in the CMS) are presented in Table 7 and Figs. 8b-8f. The description of the data at $q_0 < 0.3$ GeV and 0.6 GeV is better than that obtained by the volume-emitting Gaussian parametrizations discussed in Subsect. 3.1 or that of string-like models described in Subsect. 3.2. At $q_0 < 0.15$ GeV, the quoted values for λ and τ_K are consistent within errors with those obtained for the pion induced data in our experiment [28]. The results obtained for τ differ, however; the reasons being that in the present work:

- i) the combined π^+/K^+ data are used;
- ii) the fraction of a given multiplicity in the reference sample is taken equal to that in the real event sample (see Sect.3),
- iii) an overall normalization is used for the two-dimensional plot (Fig. 8), while in [28] 5 slices of the two-dimensional plot are normalized independently,
- iv) a background factor $(1 + \delta q_T + \epsilon q_0)$ is introduced in (7) (absent in [28]).

The confidence level of the fit is low (1.1%), particularly due to the low value of the model prediction at low q_0 and q_T (see Figs. 8a and 8b) consistent with the power-law behavior observed in [31]. The averaged parameters characterizing the space-time structure of the source are estimated to be $\tau_K = 1.44 \pm 0.18$ fm, $c\tau = 1.2 \pm 0.2$ fm, $\lambda = 0.42 \pm 0.04$. The quoted errors include the dispersion of the parameters due to different ranges of q_0 .

Note that, despite the satisfactory description of the data with parametrization (7), the extracted parameter τ_K should be considered as a mean radius of the source approximated by a spherically-symmetric form. The fit results according to (7) at different intervals of angle θ between the vector \mathbf{q} and the collision axis are presented in Table 8. One can see that the longitudinal size of the source (at $|\cos \theta| > 0.7$) exceeds the transverse one (at $|\cos \theta| < 0.3$). The dependence of BEC on the orientation of \mathbf{q} observed recently in [28,29,41,42] also grants a prolate form of the particle emitting region. Note the extracted value τ of the mean radiation time also reveals angular dependence. Contrary to τ_K , however, it decreases with increasing $|\cos \theta|$ (see also [28]).

4 SUMMARY

Bose-Einstein correlations have been studied in two and three dimensions for pairs of negative pions in $(\pi^+/K^+)p$ -interactions at 250 GeV/c.

In the variables q^2 and q_0^2 , our data exclude a volume-emitting fireball-like spherically symmetric source with a Gaussian space-time distribution (parametrization (1)). Contrary to data from e^+e^- and μN collisions, our data, furthermore, cannot be described as a function of the single variable $Q^2 = q^2 - q_0^2$ and are thus inconsistent with parametrization (2). The space-time evolution of multiparticle production, therefore, is different in hadron- and lepton-induced reactions.

Our data do not confirm the expectation from the string type model [10], which predicts an exponential rise of the BE correlation function in the region of negative Q_L^2 (parametrization (3)). Comparatively more successful is the description in the variables $|Q_L^2|$ and Q_T^2 used in the framework of the string model developed in [8].

A good description of our data is, however, achieved in the framework of the hydrodynamical expanding source model. The two-dimensional analysis (parametrization (5)) reveals the y - and m_T -dependence of the longitudinal interferometric radius r_L predicted by the model (formula (8)). The proper freeze-out time of hadronic matter is estimated to be $c\tau_f = 1.3 \pm 0.2$ fm (at $T_f = 140$ MeV). The three-dimensional analysis (parametrization (6)) leads to the relation $r_L > r_o > r_s$, with the 'side' radius (assumed to measure the geometrical transverse size of the hydrodynamical tube) $r_s = 0.76 \pm 0.10$ fm. An indication is obtained that in meson-proton collisions the pion radiation occurs during earlier stages of matter evolution and at higher densities than in nuclear collisions.

Alternatively, (except for the smallest q_T and q_0) our data are also described in the framework of a non-expanding surface-emitting fireball-like source with mean radius $r_K = 1.44 \pm 0.18$ fm and mean decay time $c\tau = 1.2 \pm 0.2$ fm (parametrization (7)). The shape of the fireball is found to be prolate rather than spherically symmetric.

Acknowledgments

We are grateful to the III. Physikalisches Institut B, RWTH Aachen, Germany, the DESY-Institut für Hochenergiephysik, Berlin-Zeuthen, Germany; the Department of High Energy Physics, Helsinki University, Finland; the Institute for High Energy Physics, Protvino, Russia; and the University of Warsaw and Institute of Nuclear Problems, Poland for early contributions to this experiment. We thank T. Csörgő for a number of important comments. This work is part of the research program of the "Stichting voor Fundamenteel Onderzoek der Materie (FOM)", which is financially supported by the "Nederlandse Organisatie voor Wetenschappelijk Onderzoek (NWO)". We further thank NWO for support of this project within the program for subsistence to the former Soviet Union (07-13-038). The work is partially supported by the Polish KBN grant no. 2 P03B 083 08 and by the Polish-German Collaboration Foundation FWPN no. 1441/LN/94.

References

- [1] W.A. Zajc: Proc. Hadronic Multiparticle Production, ed. P. Carruthers (World Scientific, Singapore, 1988) p. 235
- [2] M.I. Podgoretzkiĭ: Sov. J. Part. Nucl. 20 (1989) 266
- [3] B. Lörstad: Int. J. Mod. Phys. A4 (1989) 2861
- [4] D.H. Boal, C.-K. Gelbke, B.K. Jennings: Rev. Mod. Phys. 62 (1990) 553
- [5] E.A. De Wolf: Proc. XXIV Int. Symp. on Multiparticle Dynamics, Vietri sul Mare (Italy) 1994, eds. A. Giovannini, S. Lupia and R. Ugoccioni (World Scientific, Singapore, 1995) p. 15
- [6] X. Artru, G. Mennessier: Nucl. Phys. B70 (1974) 93
- [7] J.D. Bjorken: Phys. Rev. D27 (1983) 140
- [8] M.G. Bowler: Z. Phys. C29 (1985) 617
- [9] B. Andersson, W. Hofmann: Phys. Lett. B169 (1986) 364
- [10] M.G. Bowler: Proc. of Int. Work. on Correlation and Multiparticle Production (LESIP IV), Marburg, 1990, eds. M. Plümer, S. Raha and R.M. Weiner (World Scientific, Singapore, 1991) p.2
- [11] S. Pratt: Phys. Rev. Lett. 53 (1984) 1219
- [12] K. Kolehmainen, M. Gyulassy: Phys. Lett. B180 (1986) 203
- [13] G. Bertsch, M. Gong, M. Tohyana: Phys. Rev. C37 (1988) 1896
- [14] V.A. Averchenkov, A.N. Makhlin, Yu.M. Sinyukov: Yad.Fiz. 46 (1987)1525
A.N. Makhlin, Yu.M. Sinyukov: Z. Phys. C39 (1988) 69
- [15] Yu.M. Sinyukov: Nucl. Phys. A498 (1989) 151c
- [16] G.F. Bertsch: Nucl. Phys. A498 (1989) 173c
- [17] S.S. Padula, M. Gyulassy, S. Gavin: Nucl. Phys. B329 (1990) 357
- [18] S. Pratt, T. Csörgő, J. Zimani: Phys. Rev. C46 (1990) 2646
- [19] B. Lörstad, Yu.M. Sinyukov: Phys. Lett. B265 (1991) 159
- [20] J. Bolz et al.: Phys. Rev. D49 (1993) 3860
- [21] S.V. Akkelin, Yu.M. Sinyukov: Preprint ITP-63-94E, 1994, Kiev.
- [22] S. Chapman, P. Scotto, U. Heinz: Phys. Rev. Lett. 74 (1995) 4400
- [23] T. Csörgő: Phys. Lett. B347 (1995) 354
T. Csörgő, B. Lörstad: "Bose-Einstein Correlations for Three-Dimensionally Expanding Cylindrically Symmetric Finite Systems", Preprint LUNFD6/(NFFL-7082) 1994
- [24] G. Goldhaber et al.: Phys. Rev. Lett. 3 (1959) 181 and Phys. Rev. 120 (1960) 300
- [25] G.I. Kopylov, M.I. Podgoretzkiĭ: Sov. J. Nucl. Phys. 15 (1972) 219; 18 (1974) 336; G.I. Kopylov: Phys. Lett. B50 (1974) 472
- [26] M. Aguilar-Benitez et al.: Nucl. Instr. and Meth. 205 (1983) 79
- [27] M. Adamus et al., NA22 Coll.: Z. Phys. C37 (1988) 347
- [28] N.M. Agababyan et al., NA22 Coll.: Z. Phys. C59 (1993) 195
- [29] N.M. Agababyan et al., NA22 Coll.: Z. Phys. C66 (1995) 409
- [30] N.M. Agababyan et al., NA22 Coll.: Z. Phys. C68 (1995) 229
- [31] N.M. Agababyan et al., NA22 Coll.: Z. Phys. C59 (1993) 405
- [32] M. Althoff et al., TASSO Coll.: Z. Phys. C30 (1986) 355
- [33] M.R. Adams et al., E665 Coll.: Phys. Lett. B308 (1993) 418
- [34] T. Åkesson et al., AFS Coll.: Z. Phys. C36 (1987) 517
- [35] D. Ferenc et al., NA35 Coll.: Nucl. Phys. A544 (1992) 531c
- [36] K. Baker et al., NA44 Coll.: Z. Phys. C64 (1994) 209 and Phys. Rev. Lett. 74 (1995) 3340
- [37] T. Alber et al., NA35 Coll.: Z. Phys. C66 (1995) 77
- [38] T. Csörgő and S. Pratt: Proc. Workshop on Relativistic Heavy Ion Physics at Present and Future Accelerators, eds. T. Csörgő et al., KFKO-1991-28/A (1991) p. 75
- [39] T. Csörgő and B. Lörstad: Nucl. Phys. A590 (1995) 465c
- [40] J.D. Bjorken: Proc. XXIV Int. Symp. on Multiparticle Dynamics, Vietri sul Mare (Italy) 1994, eds. A. Giovannini, S. Lupia and R. Ugoccioni (World Scientific, Singapore, 1995) p. 579
- [41] T. Åkesson et al., AFS Coll.: Phys. Lett. B187 (1987) 420
- [42] R.A. Kvatadze, R. Møller, B. Lörstad: Z. Phys. C38 (1988) 551

FIGURE CAPTIONS

- Fig. 1 The momentum components in the transverse momentum plane.
- Fig. 2 a) Lego plot for the ratio $R(\mathbf{q}^2, q_0^2)$ at $\mathbf{q}^2, q_0^2 < 0.5 \text{ GeV}^2$; b) at $\mathbf{q}^2, q_0^2 < 2.5 \text{ GeV}^2$; c) the ratio $R(\mathbf{q}^2, q_0^2)$ as a function of \mathbf{q}^2 at $\mathbf{q}^2 \approx q_0^2$; d) as a function of Q^2 at $\mathbf{q}^2, q_0^2 > 0.8 \text{ GeV}^2$.
- Fig. 3 a) Lego plot for the ratio $R(Q_L^2, Q_T^2)$ at $-0.5 \leq Q_L^2 \leq 0.5 \text{ GeV}^2$ and $0 \leq Q_T^2 \leq 0.5 \text{ GeV}^2$ and (b-p) its slices in different intervals of Q_T^2 . The curves are the fit results obtained according to parametrization (3).
- Fig. 4 a) Lego plot for the ratio $R(|Q_L^2|, Q_T^2)$ at $0 \leq |Q_L^2| \leq 0.5 \text{ GeV}^2$ and $0 \leq Q_T^2 \leq 0.5 \text{ GeV}^2$ and (b-p) its slices in different intervals of Q_T^2 . The curves are the fit results obtained according to parametrization (4).
- Fig. 5 a) Lego plot for the ratio $R(q_L, Q_T)$ at $0 \leq q_L \leq 1 \text{ GeV}$ and $0 \leq Q_T \leq 1 \text{ GeV}$ and (b-h) its slices in different intervals of Q_T . The curves are the fit results obtained according to parametrization (5).
- Fig. 6 The y -dependence of r_L in the a) CMS and b) LCMS frames, obtained with parametrization (5). The dashed curve is the function $r_L(0)/\text{ch}y$.
- Fig. 7 The projections of the ratio $R(q_L, Q_{T_0}, Q_{T_s})$ onto the three axes with 40 MeV cuts on the non-projected components. The curves are the fit results obtained according to parametrization (6).
- Fig. 8 a) Lego plot for the ratio $R(q_T, q_0)$ at $0 \leq q_T \leq 1 \text{ GeV}$ and $0 \leq q_0 \leq 0.6 \text{ GeV}$ and (b-f) its slices in different intervals of q_0 . The curves are the fit results obtained according to parametrization (7).

Table 1: Fit results according to parametrization (1) to the ratio R as a function of q^2 and q_0^2 , for different ranges and binnings

range of variables, GeV^2	binning of variables, GeV^2	γ	λ	β_1, GeV^{-2}	β_2, GeV^{-2}	δ, GeV^{-2}	$\epsilon, \text{GeV}^{-2}$	χ^2/NDF	CL (%)
0-0.5	0.02	1.135 ± 0.015	0.451 ± 0.027	20.58 ± 2.11	-2.92 ± 2.19	-0.244 ± 0.037	0.010 ± 0.035	386/319	0.5
0-2.5	0.1	1.007 ± 0.007	0.377 ± 0.015	7.37 ± 0.47	-2.74 ± 0.66	-0.024 ± 0.005	-0.052 ± 0.006	360/319	5.

Table 2: Fit results according to parametrization (3) to the ratio R as a function of Q_L^2, Q_T^2 for different ranges of Q_L^2 (at $Q_T^2 < 0.5(\text{GeV}/c)^2$)

range of variables, GeV^2	γ	λ	β_L, GeV^{-2}	β_T, GeV^{-2}	δ, GeV^{-2}	$\epsilon, \text{GeV}^{-2}$	χ^2/NDF	CL (%)
$-0.5 \leq Q_L^2 \leq 0.5$	0.879 ± 0.007	0.454 ± 0.024	5.65 ± 0.76	5.27 ± 0.74	0.029 ± 0.098	0.025 ± 0.126	1837/929	< 0.001
$0 \leq Q_L^2 \leq 0.5$	0.729 ± 0.024	0.707 ± 0.055	6.50 ± 0.44	2.38 ± 0.21	0.450 ± 0.067	0.229 ± 0.042	1077/619	< 0.001
$-0.5 \leq Q_L^2 \leq 0$	no fit							

Table 3: Fit results according to parametrization (4) to the ratio R as a function of Q_L^2 and Q_T^2 for different ranges of Q_L^2 (at $Q_T^2 \leq 0.5 \text{ GeV}^2$)

range of Q_L^2 GeV^2	γ	A	β_L, GeV^{-2}	β_T, GeV^{-2}	δ GeV^{-2}	ϵ GeV^{-2}	χ^2/NDF	CL (%)
$-0.5 \leq Q_L^2 \leq 0.5$	0.982 ± 0.010	0.346 ± 0.021	8.80 ± 1.31	7.85 ± 0.61	-0.225 ± 0.018	-0.001 ± 0.027	1083/929	0.05
$0 \leq Q_L^2 \leq 0.5$	0.864 ± 0.035	0.292 ± 0.022	3.63 ± 1.34	3.91 ± 0.38	0.041 ± 0.054	0.179 ± 0.057	1084/619	< 0.001
$-0.5 \leq Q_L^2 \leq 0$	no fit							
$0 \leq Q_L^2 \leq 0.5$	0.992 ± 0.013	0.371 ± 0.025	10.08 ± 1.74	9.34 ± 0.82	-0.259 ± 0.026	0.067 ± 0.028	678/621	5.

Table 4: Fit results according to parametrization (5) of the ratio R as a function of q_L and Q_T , for $|Y| < 1.5$

γ	λ	τ_L, fm	τ_T, fm	δ GeV^{-1}	ϵ GeV^{-1}	χ^2/NDF	CL (%)
0.968 ± 0.011	0.471 ± 0.021	1.23 ± 0.06	0.89 ± 0.04	-0.184 ± 0.010	0.047 ± 0.013	603/619	63

Table 5: Fit results according to parametrization (5) of the ratio R as a function of q_L , Q_T for different ranges of $\langle m_T \rangle$

range of m_T GeV	γ	λ	r_l , fm	r_T , fm	δ GeV $^{-1}$	ϵ GeV $^{-1}$	χ^2 /NDF	CL (%)	$r_L \sqrt{\langle m_T \rangle}$ fm · GeV $^{1/2}$	$r_T \sqrt{\langle m_T \rangle}$ fm GeV $^{1/2}$
< 0.35	0.975 ± 0.014	0.499 ± 0.025	1.32 ± 0.06	0.98 ± 0.04	-0.184 ± 0.013	0.097 ± 0.021	711/615	0.4	$0.67 \pm 0.07^*$	$0.50 \pm 0.05^*$
0.35-1	0.910 ± 0.034	0.366 ± 0.046	0.99 ± 0.13	0.65 ± 0.07	-0.170 ± 0.025	0.232 ± 0.039	616/619	54	$0.66 \pm 0.11^*$	$0.44 \pm 0.07^*$

* errors include the dispersion in m_T

Table 6: Fit results according to parametrization (6) of the ratio R as a function of q_L , Q_{T0} and Q_{Ts} for $|Y| < 1.5$ and $0 < q_L, Q_{T0}, Q_{Ts} < 0.6$ GeV

n_{ch}	γ	λ	r_L , fm	r_o , fm	r_s , fm	$r_{o,L}$, fm	δ GeV $^{-1}$	ϵ GeV $^{-1}$	ξ GeV $^{-1}$	χ^2 /NDF	CL (%)
all	1.073 ± 0.015	0.244 ± 0.024	1.89 ± 0.23	1.28 ± 0.15	0.75 ± 0.10	0.81 ± 0.34	-0.313 ± 0.020	-0.068 ± 0.019	-0.239 ± 0.016	3400/3366	7
all	1.075 ± 0.015	0.247 ± 0.024	1.75 ± 0.20	1.18 ± 0.13	0.76 ± 0.10	0.0	-0.315 ± 0.020	-0.067 ± 0.019	-0.240 ± 0.016	3491/3367	7
< 10	0.929 ± 0.100	0.245 ± 0.088	1.41 ± 0.26	1.06 ± 0.23	0.68 ± 0.12	0.0	-0.411 ± 0.102	-0.035 ± 0.090	-0.177 ± 0.074	3658/3367	0.02
≥ 10	1.087 ± 0.015	0.236 ± 0.025	1.81 ± 0.21	1.23 ± 0.14	0.79 ± 0.11	0.0	-0.321 ± 0.020	-0.086 ± 0.019	-0.260 ± 0.017	3562/3367	1

Table 7: Fit results according to parametrization (7) of the ratio R as a function of q_T and q_0 for different ranges of q_0 (at $q_T \leq 1$ GeV)

range of q_0 GeV	γ	λ	r_K , fm	$c\tau$, fm	δ GeV $^{-1}$	ϵ GeV $^{-1}$	χ^2 /NDF	CL (%)
0-0.15	1.151 ± 0.026	0.423 ± 0.035	1.54 ± 0.08	1.30 ± 0.18	-0.183 ± 0.026	-0.090 ± 0.094	240/194	1.1
0-0.30	1.133 ± 0.023	0.422 ± 0.028	1.45 ± 0.07	1.23 ± 0.12	-0.167 ± 0.022	-0.074 ± 0.037	406/394	35.
0-0.60	1.130 ± 0.015	0.425 ± 0.022	1.44 ± 0.06	1.13 ± 0.09	-0.155 ± 0.014	-0.114 ± 0.015	820/794	26.

Table 8: Fit results according to parametrization (7) of the ratio R as a function of q_T and q_0 for different ranges of q_0 (at $q_T \leq 1$ GeV)

range of q_0 GeV	$ \cos\theta $	γ	λ	r_K , fm	$c\tau$, fm	δ GeV $^{-1}$	ϵ GeV $^{-1}$	χ^2 /NDF	CL (%)
0-0.15	0-0.3	1.049 ± 0.060	0.417 ± 0.073	1.49 ± 0.17	1.71 ± 0.40	-0.245 ± 0.064	0.128 ± 0.192	240/194	1
	0.3-0.7	1.045 ± 0.052	0.386 ± 0.052	1.43 ± 0.14	1.44 ± 0.34	-0.200 ± 0.047	-0.071 ± 0.158	237/194	1.5
	0.7-1	1.058 ± 0.035	0.500 ± 0.065	1.72 ± 0.12	1.09 ± 0.27	-0.141 ± 0.039	-0.137 ± 0.155	228/194	4.5
0-0.30	0-0.3	0.989 ± 0.093	0.468 ± 0.102	1.30 ± 0.20	1.50 ± 0.29	-0.152 ± 0.097	-0.052 ± 0.142	473/394	0.3
	0.3-0.7	1.022 ± 0.052	0.383 ± 0.057	1.31 ± 0.13	1.29 ± 0.23	-0.178 ± 0.053	-0.027 ± 0.077	429/394	12
	0.7-1	1.060 ± 0.028	0.457 ± 0.048	1.67 ± 0.11	0.95 ± 0.14	-0.150 ± 0.030	-0.105 ± 0.054	409/394	30
0-0.60	0-0.3	1.023 ± 0.037	0.425 ± 0.051	1.35 ± 0.12	1.46 ± 0.21	-0.170 ± 0.039	-0.179 ± 0.041	1003/794	0.001
	0.3-0.7	1.051 ± 0.025	0.359 ± 0.037	1.36 ± 0.11	1.43 ± 0.21	-0.209 ± 0.024	-0.043 ± 0.029	826/794	21
	0.7-1	1.057 ± 0.020	0.439 ± 0.038	1.59 ± 0.09	0.87 ± 0.10	-0.141 ± 0.020	-0.134 ± 0.020	826/794	21

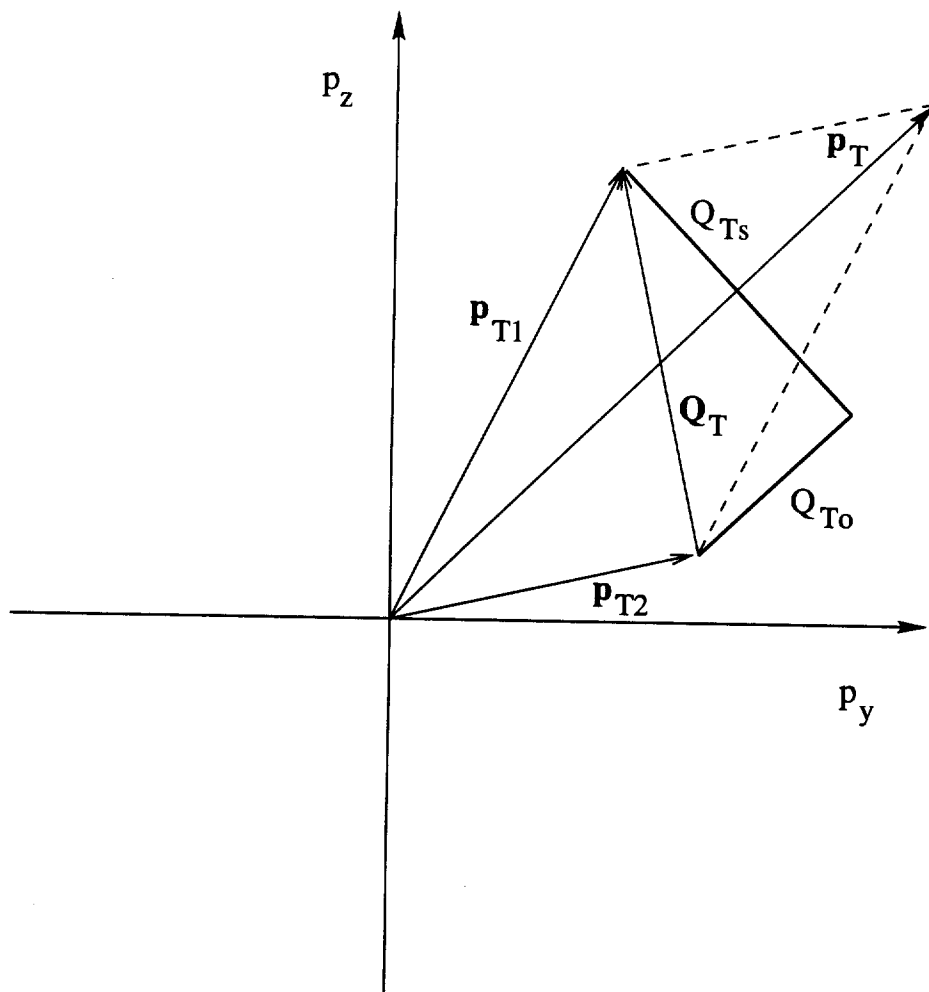


Fig. 1

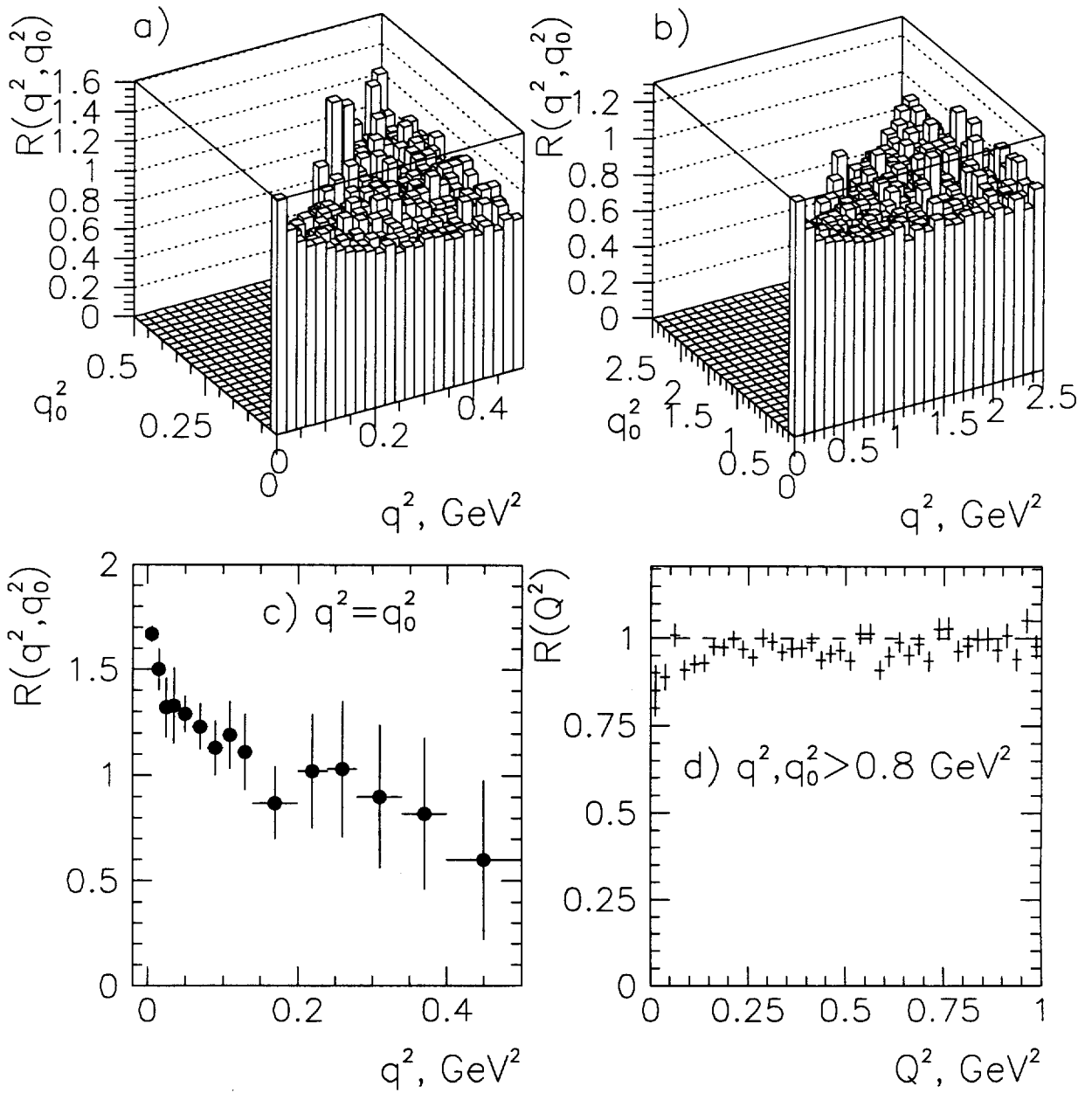


Fig. 2

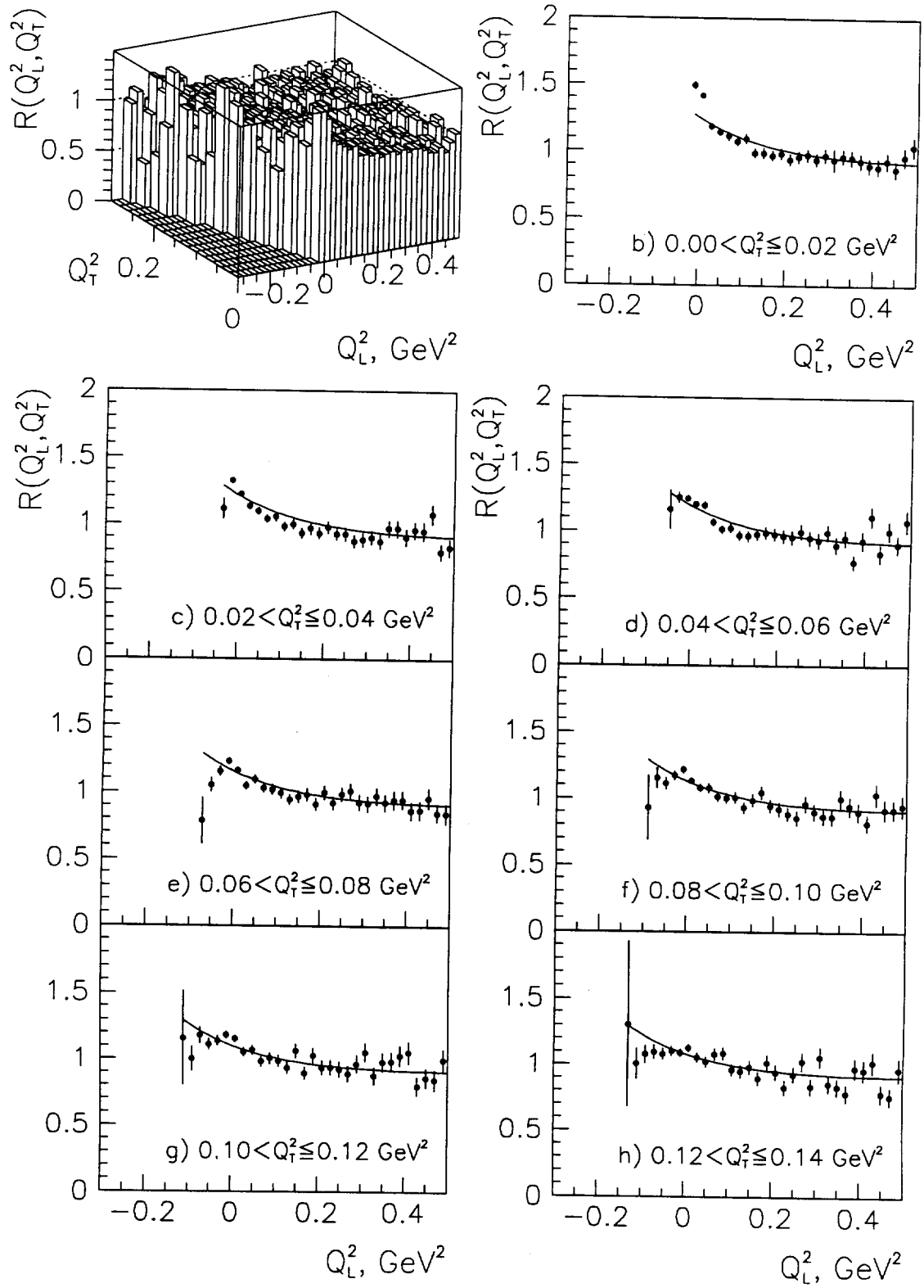


Fig. 3

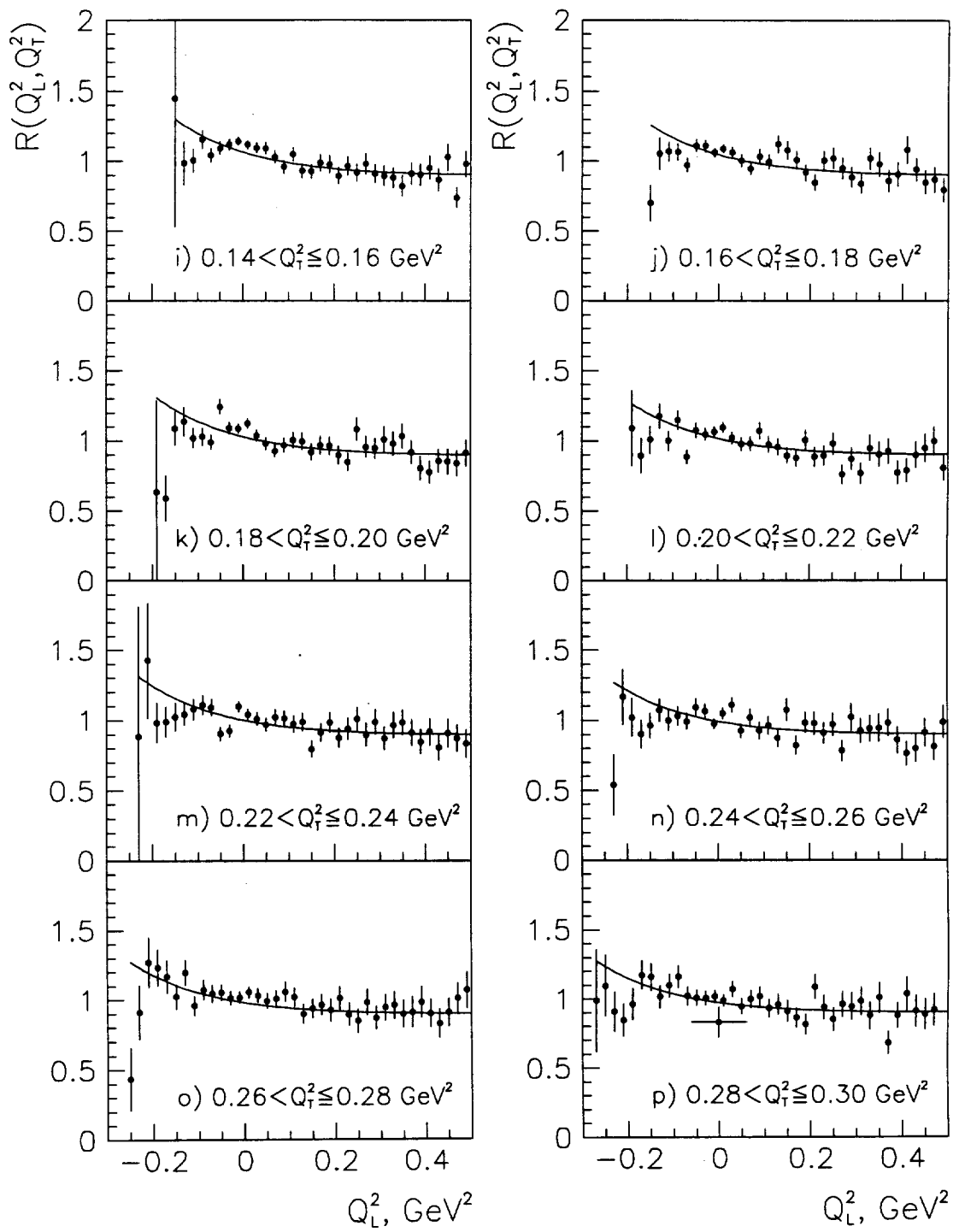


Fig. 3

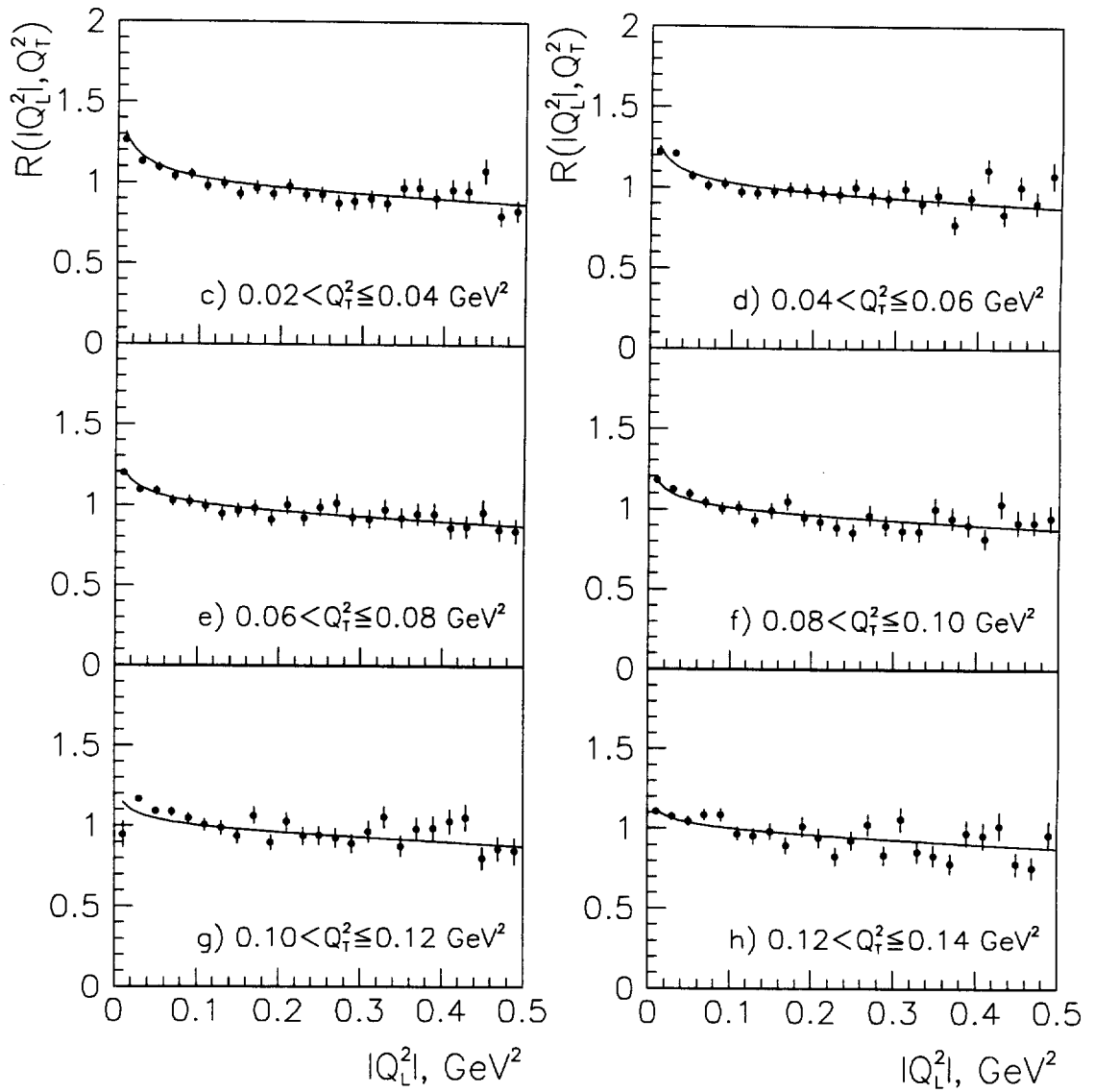
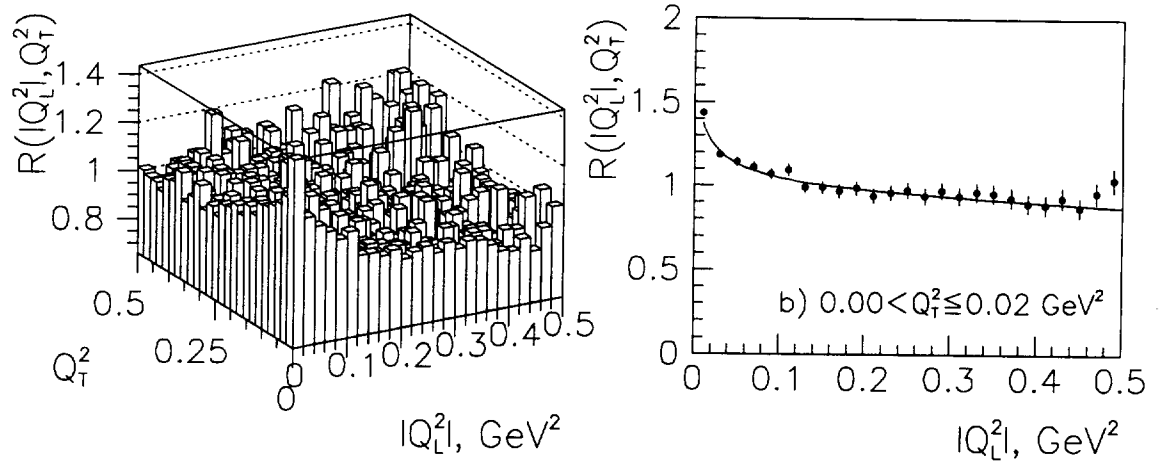


Fig. 4

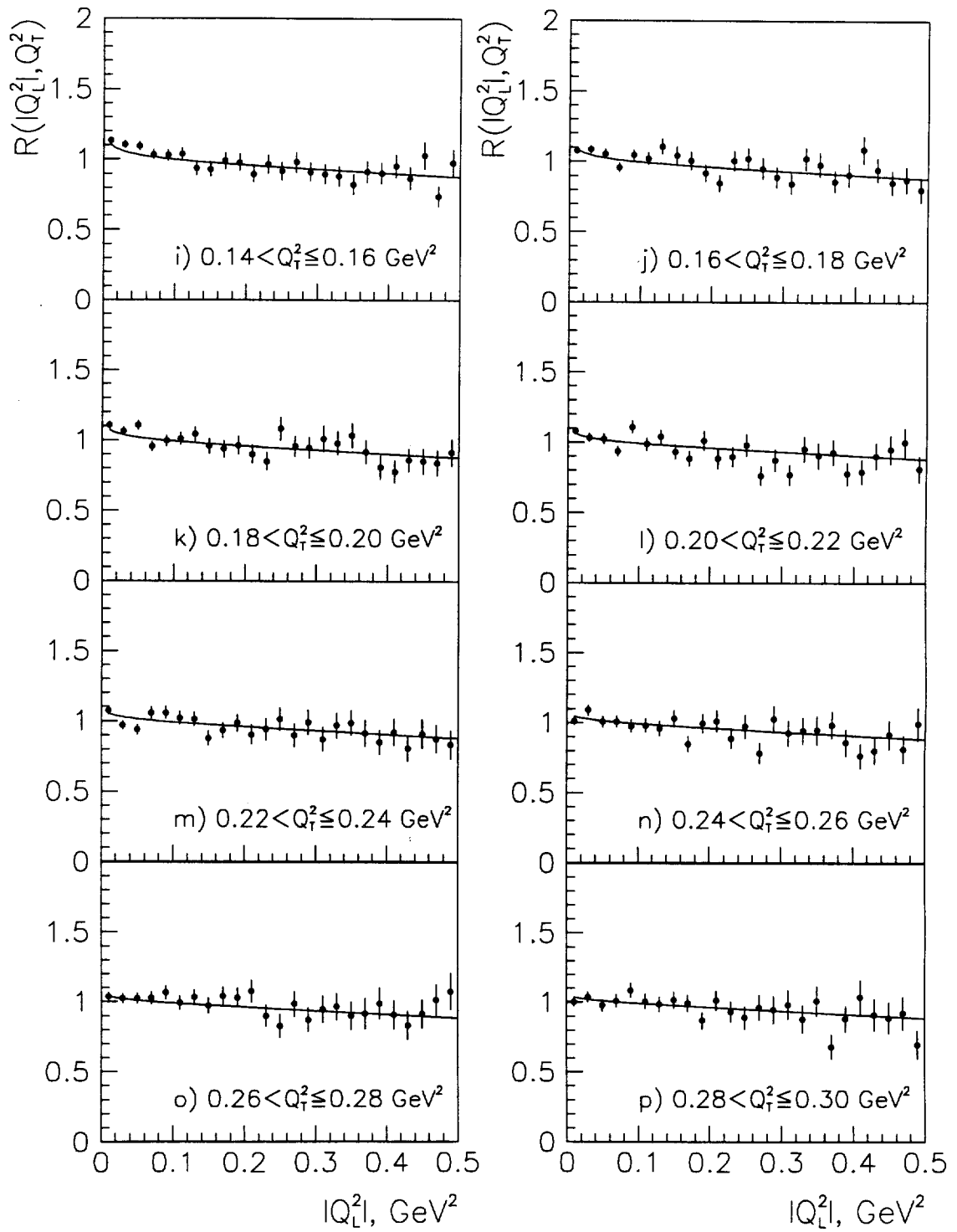


Fig. 4

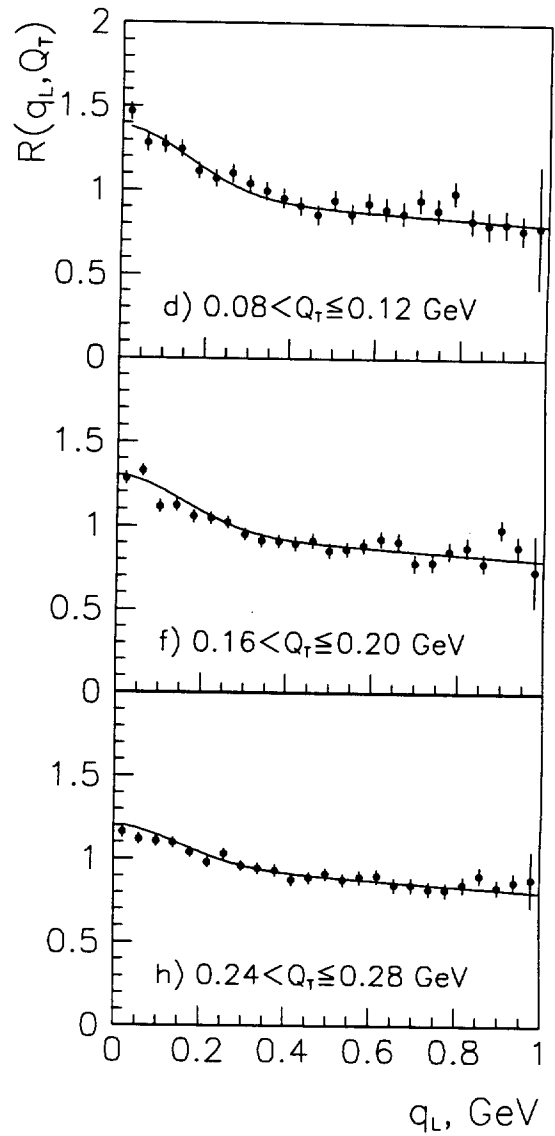
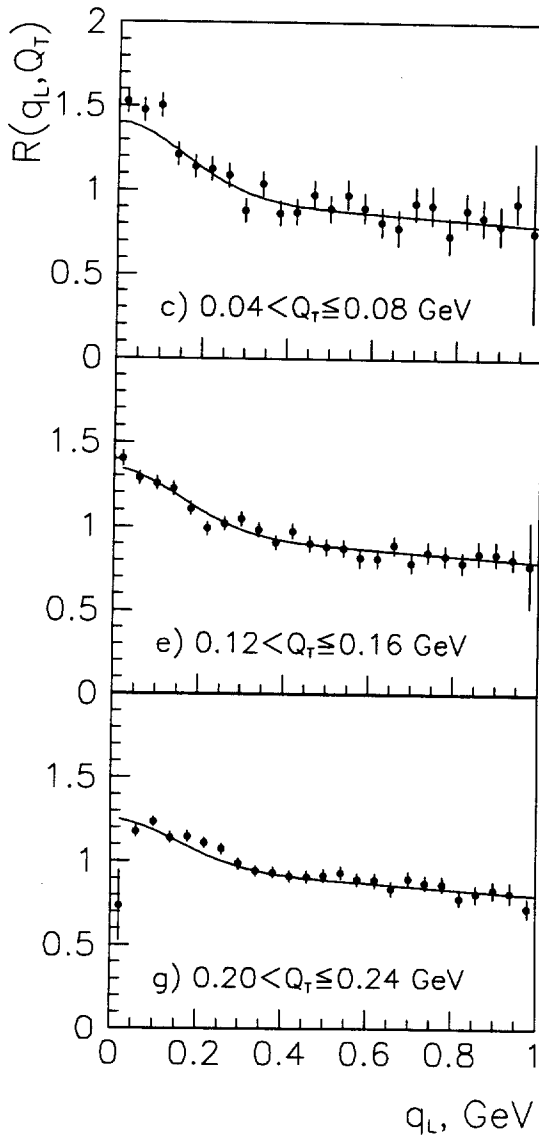
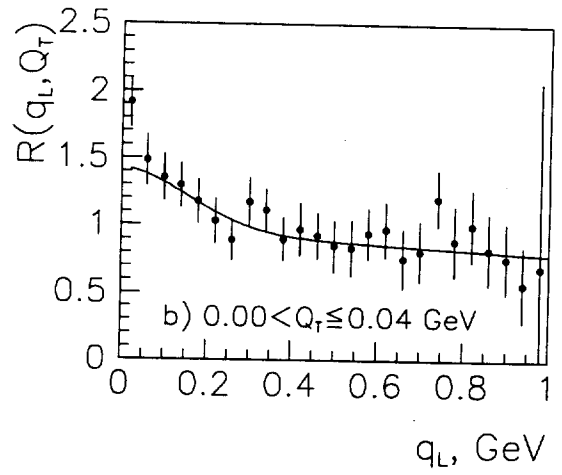
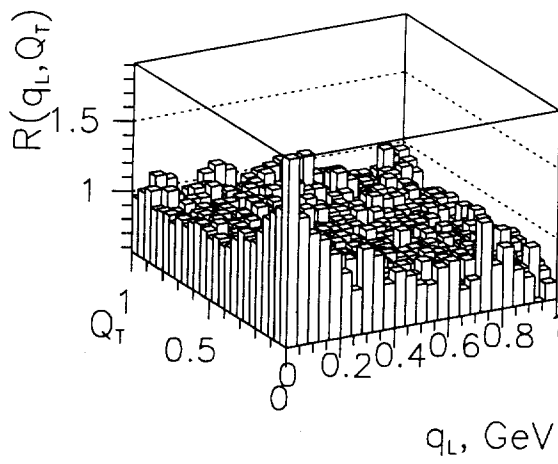


Fig.5

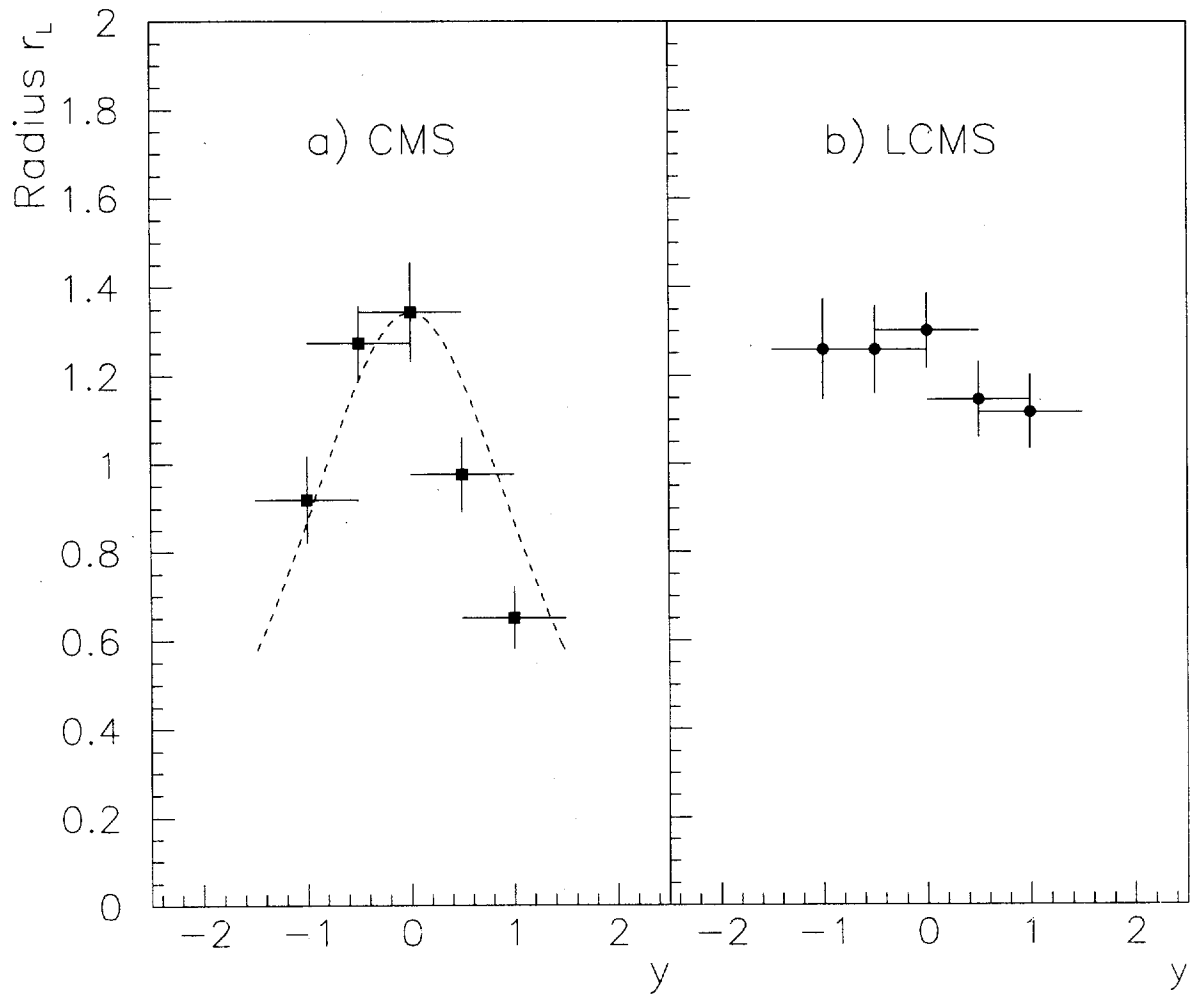


Fig. 6

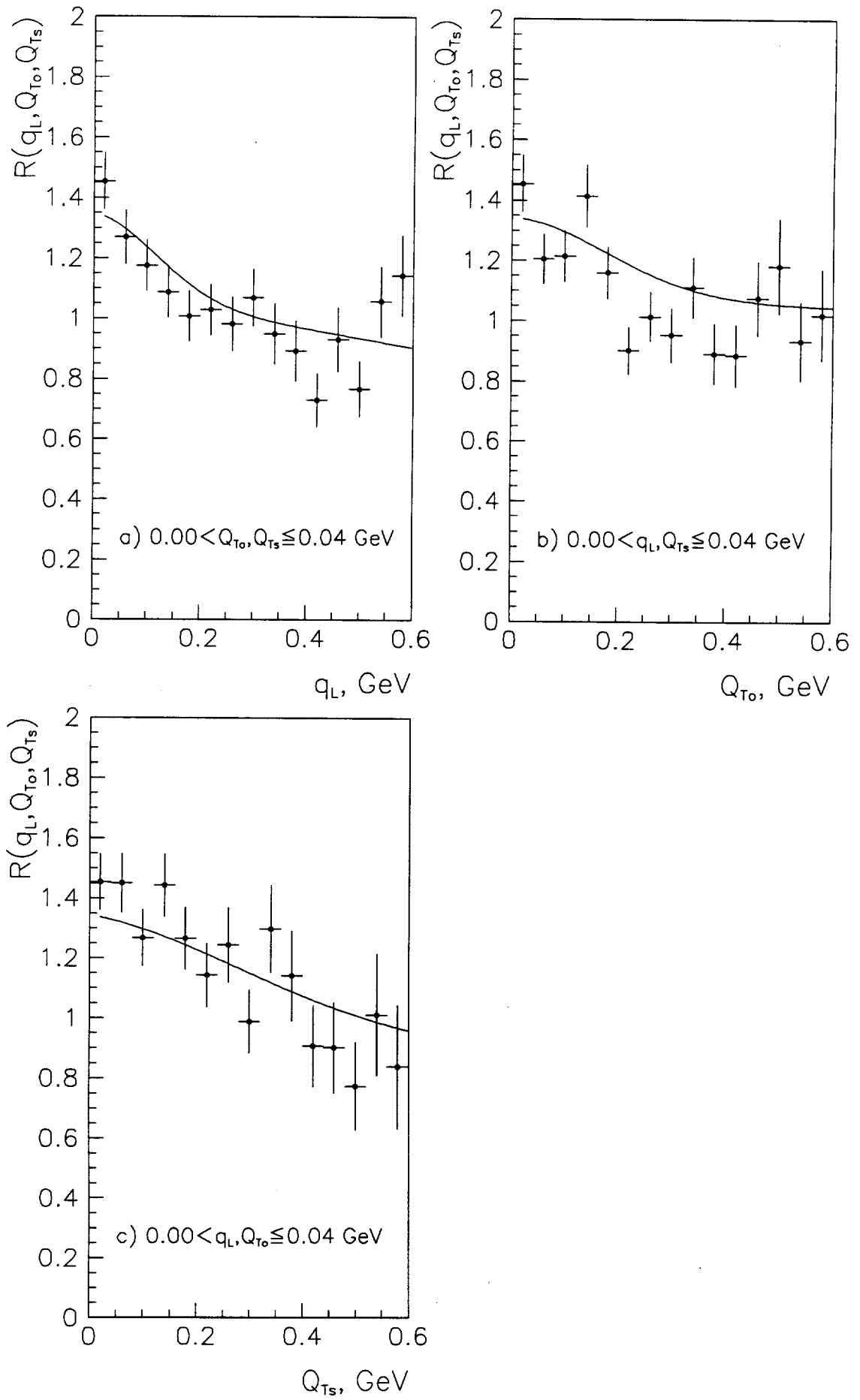


Fig.7

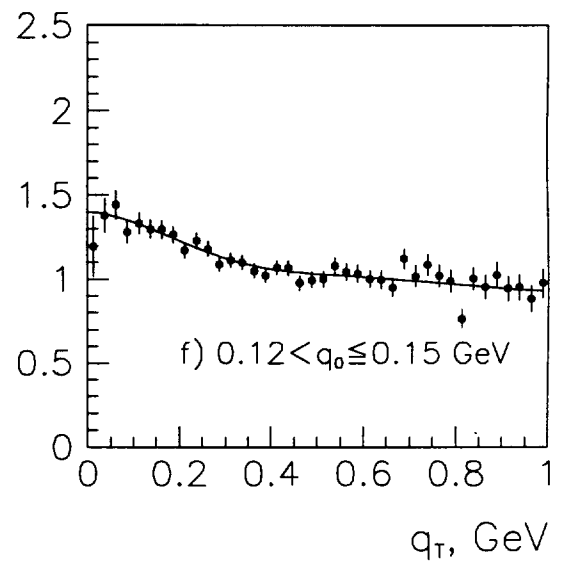
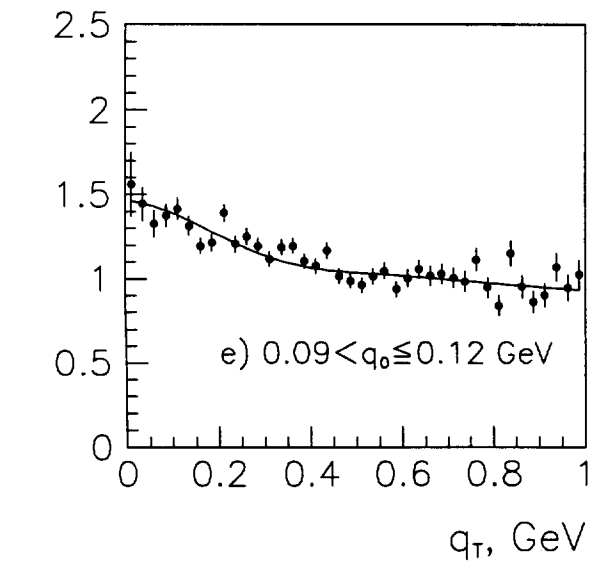
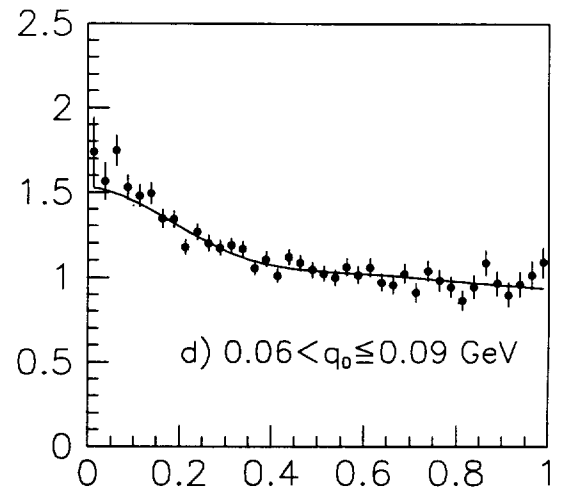
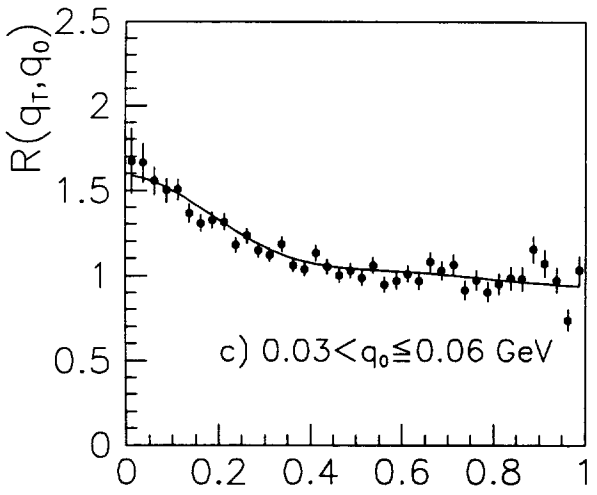
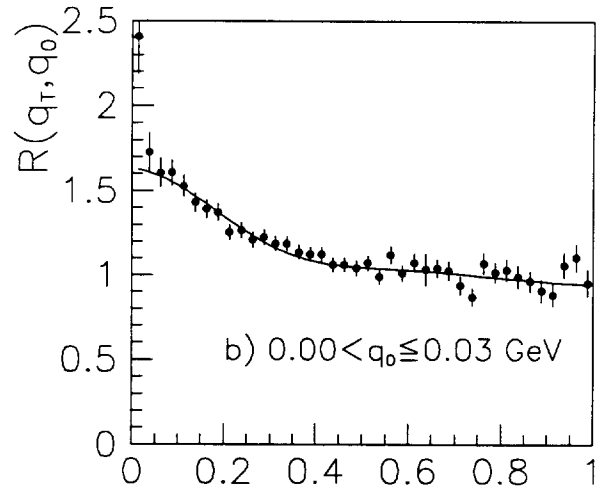
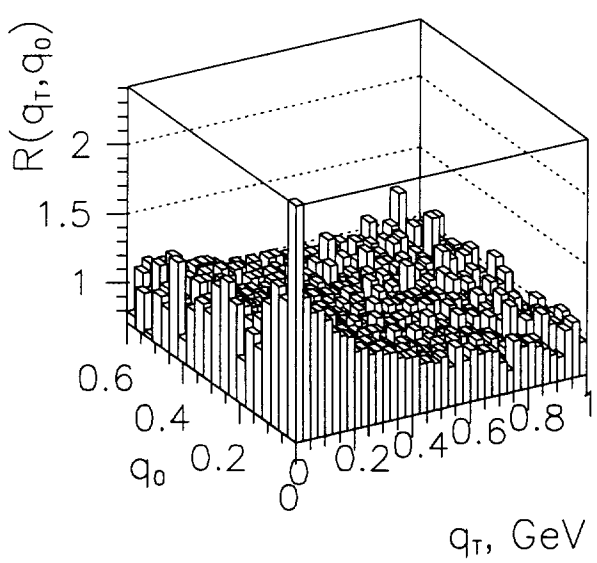


Fig.8

